# Experimental Investigation of the Oil Jet Heat Transfer on a Rotating Cylinder for an Aero Engine Gearbox

**Christian Kromer, Emre Ayan, Corina Schwitzke, Hans-Jörg Bauer**
**christian.kromer@kit.edu**

Institute of Thermal Turbomachinery (ITS),
Karlsruhe Institute of Technology (KIT),
Kaiserstrasse 12, 76131 Karlsruhe,
Germany

## Abstract

Geared turbofan engines have the potential to propel future civil aircraft engines more efficiently. A planetary gearbox between the low-pressure turbine and the fan enables the operation of both components at their respective optimum rotational speeds. This makes it possible to achieve higher bypass ratios and thus a better propulsion efficiency. A crucial part of the planetary gearbox design is the cooling and lubrication of the gears. Sufficient heat removal from the gear tooth flanks is necessary to ensure reliable operation without the risk of gear failure through pitting or scoring. Fast rotating and highly loaded gears are cooled with impinging oil jets according to current design guidelines. This impingement cooling process comprises a complex, multi-phase flow with heat transfer. Previous experimental, numerical and analytical investigations have shown that the cooling process depends both on the highly unsteady liquid flow dynamics and on the heat conduction in the oil film formed on the gear tooth flank. In this study, the gear is replaced by a cylinder in order to be able to study the impingement cooling on a rotating surface without the influence of unsteady flow phenomena. A hollow cylinder is instrumented with 42 thermocouples across the surface, which are all connected to a telemetry system. A single oil jet is directed radially onto the outer cylinder surface. The measured temperatures are subsequently corrected using a new algorithm to reduce systematic measurement errors without distorting the data. The corrected temperatures are used to calculate the Nusselt number distribution across the cylinder surface by means of a finite element analysis. A parameter study is performed to identify the influence of the parameters oil flow rate, oil viscosity and rotational speed of the cylinder on the heat transfer. The fundamental results of the present study enable a better understanding of the heat transfer on impingement cooled cylinders and spur gears.

**Keywords:** liquid impingement cooling, heat transfer, superposition, experimental data

## Nomenclature

**Latin**

| | | |
|---|---|---|
| $d$ | [m] | jet diameter |
| $h$ | [W/m$^2$ K] | heat transfer coefficient |
| $k$ | [W/m K] | thermal conductivity |
| $l$ | [m] | nozzle length |
| $\dot{q}$ | [W/m$^2$] | heat flux |
| $r$ | [m] | radial coordinate |
| $T$ | [K] | temperature |
| $z$ | [m] | axial coordinate with respect to impingement point |
| $\hat{z}$ | [m] | axial coordinate with respect to cylinder |

**Greek**

| | | |
|---|---|---|
| $\nu$ | [m$^2$/s] | kinematic viscosity |

**Scripts**

| | |
|---|---|
| aw | adiabatic wall |
| jet | oil jet |
| oil | oil (Mobil jet oil II) |
| TiAl | Titanium aluminum Ti-6Al-4V Grade 5 |
| w | wall |

**Similarity parameters**

| | |
|---|---|
| Nu | Nusselt number |
| Pr | Prandtl number |

**Abbreviations**

| | |
|---|---|
| FEA | Finite Element Analysis |
| rpm | revolutions per minute |
| TC | Thermocouple |

# 1.0 INTRODUCTION

The current demand for more efficient jet engines drives the development of the geared turbofan. Even though some geared turbofan engines are already on the market today, there is still no jet engine powerful enough for the long range aircraft sector. The gearbox introduced by the geared turbofan design faces tough challenges when it comes to reliability and safety. The extremely high power transmitted from the low pressure turbine to the fan leads inevitably to high losses in the form of heat dissipation in the relatively small gearbox. Efficient cooling via state-of-the-art oil jet cooling is essential to counteract this high heat density. Additionally, the oil is a vital part of the lubrication of the gears in the meshing zones. The oil jet cooling faces with two major challenges: cooling as much as possible to avoid gear failures and as little as possible to avoid churning losses. A detailed understanding of the heat transfer mechanism from the oil jets impinging on the rotating gears is, therefore, crucial.

Although oil jet cooling has been applied for a long time, most designs lean heavily on rough design guidelines and testing rather than building on a deeper understanding and modeling the thermal behavior thoroughly. This is mainly because of the absence of reliable and validated correlations for the heat transfer in the literature. This problem has been tackled in the last years with analytical models [1–3], numerical simulations [4–6] as well as experiments [7, 8] at the Institute of Thermal Turbomachinery. The experimental results published by von Plehwe et al. show complex dependencies between the heat transfer and the input parameters such as rotational

speed and oil flow rate. It is concluded that there are several effects that are superimposed on one another each, affecting the heat transfer. It can be distinguished between geometrical effects of the gear such as the impingement depth, the pulsating nature of the heat transfer generated by the gear teeth cutting the oil jet and the impingement cooling of a rotating body stemming from the rotation of the gear. For a better understanding of these underlying effects, the gear is simplified to a cylinder in this study to eliminate the pulsating effects as well as geometrical effects. The study should reveal the parameters governing the heat transfer and the results can subsequently be transferred back to the cooling of gears. This can either be achieved by introduction in analytical models [3] or in semi-empirical correlations based on the experiments [7].

# 2.0 THEORETICAL BACKGROUND

In this section, a short literature review is presented regarding oil jet impingement. First and foremost, only liquid jet impingement is considered, to be more specific, only free surface liquid jet impingement, as submerged jets exhibit completely different flow behavior. Additionally, impingement processes with phase transition, e.g. boiling, are neglected and only axisymmetric jets are taken into account. Webb and Ma present a very comprehensive literature review on such flows [9]. Many studies are published, including analytical derivations, on the fluid flow and heat transfer of liquid jets on stationary surfaces. The presented correlations are validated against experimental data and cover a wide range of operating conditions. The main dependencies of the heat transfer are linked to the jet Reynolds number, the Prandtl number of the fluid and the velocity profile right before impingement. The heat transfer is maximum at the impingement point and decreases with radial distance. Another important effect that has to be considered for high Prandtl number fluids such as oil is the dissipation effect in the boundary layer [10]. This might lead to significant increases in adiabatic wall temperature compared to the jet temperature. Minor effects include the surface roughness, the inclination angle of the jet and splattering [9].

The number of studies on jet impingement on moving surfaces is considerably smaller compared to stationary surfaces. One common field is the jet impingement on a rotating disc, described in detail by Carper et al. [11]. However, these flows cannot be compared to this study because of the different nature of their flow fields.

There are several studies focusing on the flow behavior of liquid jets impinging on a flat moving surface [12–17]. These flows are used for the application of liquid friction modifiers on railroad tracks. The main difference to the present study is that the surface is dry before the jet impinges, whereas the surface is already wetted with oil for a rotating cylinder. The impingement process onto an oncoming oil film is considered by Fujimoto et al. [18, 19], but only for low jet and surface velocities below 1 m/s. To the authors' knowledge, there is currently no study available in the literature on the flow behavior of a high speed oil jet onto a rotating cylinder.

The heat transfer of a liquid jet impinging on a moving surface has been studied by Zumbrunnen for planar laminar jets [20]. The flow behavior is significantly different from the present study limiting the applicability of the results. There is still a need in the literature to characterize an axisymmetric, free-surface liquid jet impingement on a rotating cylinder. This study makes a substantial contribution to bridge that gap in fundamental heat transfer processes, focusing on the dissipation effect as well as the heat transfer behavior.

# 3.0 METHODOLOGY

## 3.1 Experimental Setup

The aim of the test rig is to investigate an oil jet that impinges radially onto a rotating hollow cylinder. The direction of the heat transfer is inverted in the test rig to simplify the setup. The hot oil jet is used to heat the cylinder instead of cooling it. There is no change to the physics involved as long as the dissipation effect is considered as explained in Subsection 3.4. To be able to calculate the heat transfer of the flow, the inside of the cylinder is cooled by air jets to induce a radial temperature gradient in the rotating structure. The temperatures are then measured by thermocouples embedded in the rotor surface once stationary conditions are reached. The test rig is mainly comprised of four parts, the oil supply system, the air supply system, the rotating system and the test chamber. A more detailed description of the test rig is given by von Plehwe et al. [7] and the following section will only focus on the main components. The oil supply system provides Mobil Jet Oil II at the desired flow rate and temperature. They can be set as high as 9 l/min and 100°C for the nozzle used in this study. The air supply system cools the inside of the rotor with coolant air at a temperature of around 20°C. It can be replaced by an insulation layer to be able to measure near adiabatic conditions described in Subsection 3.4. The rotating cylinder is driven by an electric motor with a maximum speed of 6200 rpm (±0.1 %). It has an outer diameter of 260 mm, an inner diameter of 230 mm and an axial length of 90 mm. A schematic of the cylinder is depicted in Fig. 1 along with the coordinate system used in this study. The axial coordinate system fixed to the cylinder, $\hat{z}$, is indicated on the left hand side while the axial coordinate relative to the impingement point, $z$, is shown

in the middle of the schematic. The latter is symmetric with respect to the impingement point, which is why a second arrow is indicated by the dashed line. A telemetry unit is mounted in the center of the rotor to which the 42 thermocouples of type K and diameter 0.25 mm are connected. The telemetry unit sends out the temperature data to the data acquisition system and is subsequently stored at a rate of 1 Hz. The exact locations of the outside thermocouples are listed Table 1 as they are relevant in Subsection 3.3.

Table 1: Axial coordinates for the 32 thermocouples on the outside of the cylinder

| TC number | $\hat{z}$ [mm] | TC number | $\hat{z}$ [mm] | TC number | $\hat{z}$ [mm] | TC number | $\hat{z}$ [mm] |
|---|---|---|---|---|---|---|---|
| 1 | 0 | 9 | 29.95 | 17 | 45.98 | 25 | 63.73 |
| 2 | 3.67 | 10 | 32.14 | 18 | 47.99 | 26 | 67.49 |
| 3 | 7.34 | 11 | 33.99 | 19 | 50.09 | 27 | 71.25 |
| 4 | 11.12 | 12 | 35.82 | 20 | 52.01 | 28 | 74.99 |
| 5 | 14.76 | 13 | 37.94 | 21 | 53.94 | 29 | 78.84 |
| 6 | 18.75 | 14 | 40.05 | 22 | 55.92 | 30 | 82.45 |
| 7 | 22.67 | 15 | 42.08 | 23 | 58.28 | 31 | 86.25 |
| 8 | 25.95 | 16 | 43.94 | 24 | 59.92 | 32 | 90 |

The thermocouples on the outside of the cylinder are concentrated towards the middle of the cylinder, illustrated in Fig. 1 by the colored dots along the inside and outside surfaces of the cylinder. Small grooves of 0.3 mm width and 0.4 mm depth where milled into the cylinder to mount the thermocouples as close to the surface as possible without changing the surface geometry. The end of the grooves (last 20 mm) are oriented in circumferential direction to minimize the thermal gradient near the measurement tip of the thermocouple thereby maximizing measurement accuracy. A two component exopy resin (Duralco 132) was chosen for the mounting of the thermocouples. It exhibits a thermal conductivity of $k = 5.76\,\mathrm{W/m\,K}$ close to the titanium aluminum (Ti6Al4V) of the cylinder (see Eq. 1) to avoid an influence of the instrumentation on the thermal behavior of the cylinder. A calibration of the thermocouples was performed at ambient temperature after the instrumentation to minimize measurement errors. This was done by mounting copper rings on the inside and outside to ensure thermal equilibrium and recording the voltage offsets with respect to the oil nozzle thermocouple. These offsets were subsequently taken into account at every measurement.

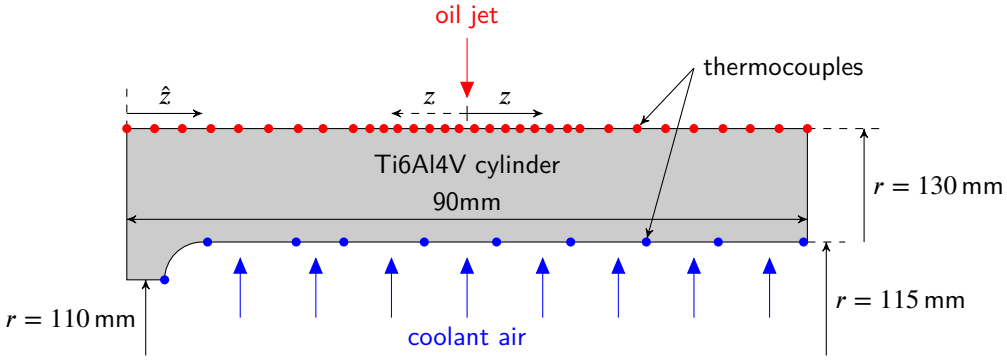


Figure 1: Schematic of the hollow cylinder at scale 1:1, cut off at the innermost thermocouple location. The thermocouple locations on the outside surface are marked by red dots, on the inside surface by blue dots.

The oil is supplied to the test rig in a tube of 10 mm diameter before it is accelerated into the 2 mm nozzle. The nozzle has a length-to-diameter ratio of $l/d = 10$ and a chamfered inlet section to avoid flow separation or cavitation. Upstream of the oil nozzle, the oil flow rate is measured using a Coriolis mass flow sensor (with a measurement error $< 0.1\,\%$), the temperature using a type T thermocouple with a diameter of 0.5 mm (accuracy of $\pm 0.5\,\mathrm{K}$) and the pressure using a membrane pressure sensor mounted flush to the side wall. In the rotating system, the rotational speed ($\pm 0.1\,\%$) and torque are measured with a torque meter. A vibration sensor is mounted near the bearing chamber to monitor the bearings and detect any possible malfunctions.

## 3.2 Measurement Procedure

The measurements are taken in the following specific order to obtain reproducible results of the best quality. Each measurement day, the test rig is heated up in a warm-up phase of about two hours to minimize heat losses

to the test chamber and the surrounding parts. Afterward, the desired operating conditions are set, including oil jet temperature, oil flow rate and rotational speed. The thermal response of the cylinder is then closely monitored until no more temperature changes can be observed. This stationary mode is kept for three minutes, of which the last 30 seconds are used in the evaluation. Thereafter, the nozzle is moved in axial direction from the middle of the cylinder at $\hat{z} = 45$ mm to $\hat{z} = 49$ mm and the measurement is repeated. The same procedure is performed another two times for the positions $\hat{z} = 41$ mm and again with the starting position of $\hat{z} = 45$ mm. The temperature data is corrected by the calibration offset recorded before the measurement campaign for each thermocouple individually. It is followed by averaging the data over 30 seconds to eliminate white noise introduced by the telemetry system. After concluding the data acquisition phase, the first and last measurement, each at the reference position of $\hat{z} = 45$ mm are compared. Only if the deviations are less then $\Delta T < 0.5$ K, the measurement is considered successful and will be evaluated further. This is done to eliminate non-stationary measurements and to detect a possible drift during the measurement campaign as the stabilization time after a nozzle movement can be as long as 30 minutes.

### 3.3 Data Correction

The calibrated data needs to be smoothed before meaningful results can be obtained. The main reason are measurement errors in combination with the small axial distance between two adjacent measurement locations. Small local measurement errors are always present in the data sets. Possible causes include measurement errors caused by the telemetry system, soldering spots, electromagnetic interference by the surrounding electronic systems like pumps and motors or the manufacturing variances in the thermocouples. The errors are all within the accuracy of the type K thermocouples of 1.5 K. An exemplary data set is plotted with blue dots in the top part of Fig. 2. The x-coordinate of the plot is the axial distance to the impingement point $z$ normalized by the jet diameter $d$.

In order to obtain the heat flux across the cylinder surface, a finite element analysis (FEA) simulation of the heat conduction in the rotor is performed using COMSOL Multiphysics v6.0. The heat conduction problem is solved with constant temperature boundary conditions. Therefore, the Laplace Equation with Dirichlet boundary condition for all boundaries has to be solved. Since the temperature is only measured at the specified local positions across the surface, a spline interpolation is used to obtain continuous temperature data for all boundaries. A two dimensional, rotationally symmetric setup is chosen for the model. The geometry is modeled according to the experimental rotor cut off at the position of the innermost thermocouple at $r = 110$ mm. The thermal conductivity of the rotor is modeled as a temperature dependent function for the material TiAl6V4 Grade 5 in the range 100-800 K [21, 22]:

$$k_{\mathrm{TiAl}} = \begin{cases} 0.1560505 + 0.07648919\,T - 2.883179 \cdot 10^{-4}\,T^2 + 3.68138 \cdot 10^{-7}\,T^3 & \text{for } T < 311\,\mathrm{K} \\ 8.114005 - 0.01485211\,T + 4.468662 \cdot 10^{-5}\,T^2 - 2.273481 \cdot 10^{-8}\,T^3 & \text{for } T \geq 311\,\mathrm{K} \end{cases} \tag{1}$$

The grid consists of 2307 quad elements with a mesh size of 1 mm along the outer boundary. The discretization scheme is of second order and the relative tolerance of the solver is set to $10^{-5}$. The resulting temperature field in the rotor is then being used to obtain the heat flux across the outer boundary where the oil jet impinges upon. This is achieved by Fourier's Law

$$\dot{q} = -k_{\mathrm{TiAl}} \frac{\partial T}{\partial r}\,, \tag{2}$$

with the fraction being the temperature gradient in radial direction.

The axial thermal conduction in the rotor leads to significant amplification of the adjacent measurement errors. The resulting heat flux distribution cannot be used for further examination. The evaluated heat flux is depicted in the bottom of Fig. 2 in blue. The underlying heat flux distribution, that we are trying to measure, is hidden because of the high levels of noise in the data.

The noise in the data can be divided into two types: white noise showing up in time-dependent data and systematic errors, that are constantly present. The first one is significantly reduced by the time-averaging and is usually in the range of only $\pm 0.25$ K. The latter one is harder to detect and eliminate, which is why a special correction algorithm is derived and explained in the following section.

An example of a systematic error and its implication on the heat flux is shown in Fig. 3 for a synthetic data set, which represents an operating condition close to the ones measured in the experiments. A synthetic data set is used to obtain a noise free temperature distribution which in turn can then be manipulated to isolate the effect of a systematic measurement error. The blue dots in the top of Fig. 3 represent the synthetic data set at the reference nozzle position (centered with respect to the axial length of the cylinder). A systematic measurement error of $+1$ K is introduced at the eleventh thermocouple counting from the left highlighted by the red arrow and the red dot. The temperature distribution after spline interpolation is plotted in green. After evaluation by means of the

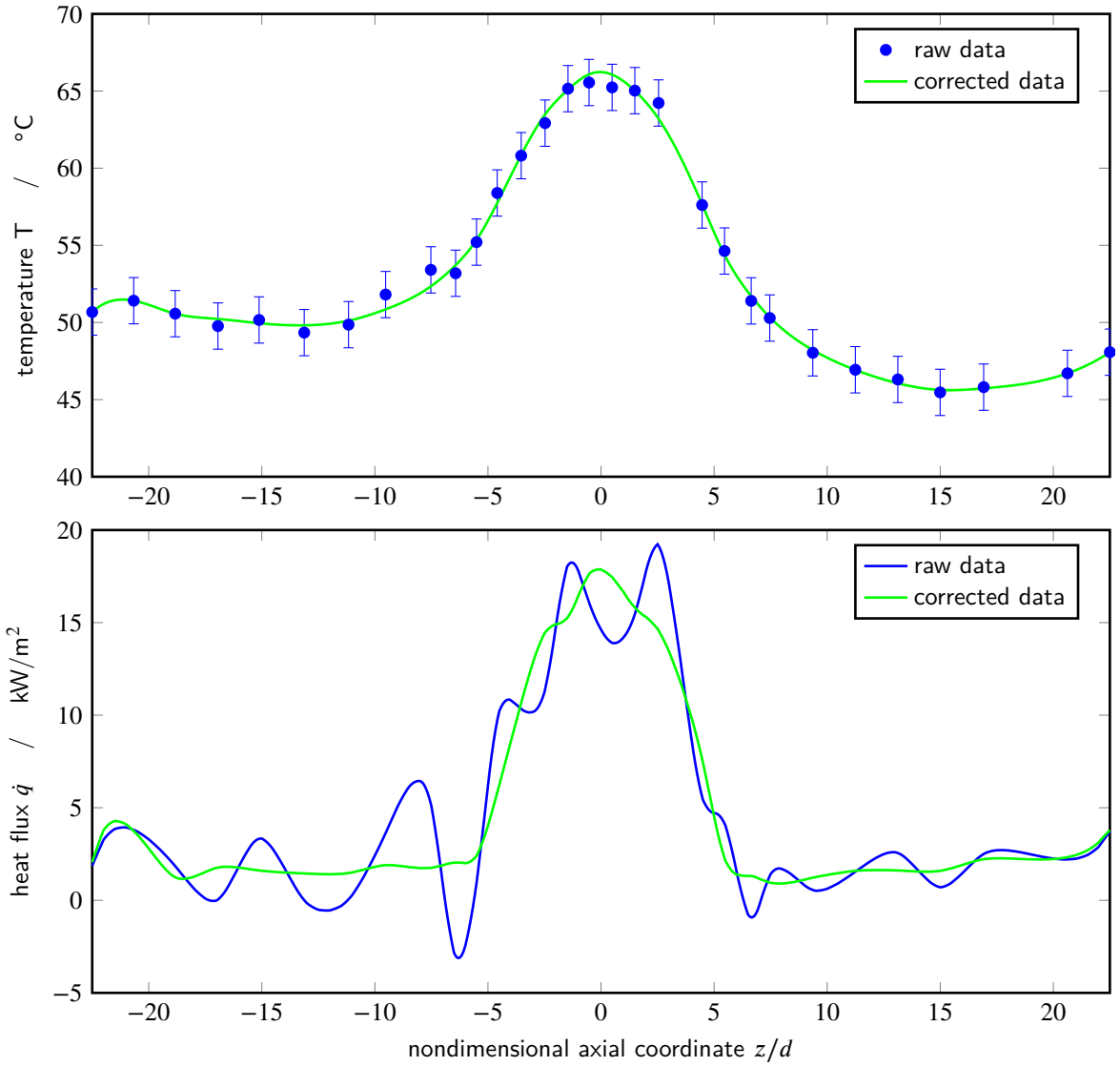


Figure 2: Top: Temperature data at the thermocouple locations before (blue) with error bars and after (green, interpolated) the correction algorithm; Bottom: Calculated heat flux before (blue) and after (green) the correction algorithm

FEA simulation, the heat flux distribution is depicted in green in the bottom of Fig. 3. Additionally, the two measurements at different nozzle positions are also shown in red and black. Please note that a positive nozzle displacement moves the heat flux distribution to the left as the nondimensional coordinate $z/d$ has its origin at the point of impingement.

There are several ways to overcome the problem of noisy measurement data. Known approaches include smoothing, e.g. via moving average, local polynomial regression or spline smoothing, or fitting, e.g. polynomial function fitting. All of these approaches have a distinct disadvantage when applied to the presented data set. Certain parameters need to be set before the data manipulation, which heavily impact the resulting heat flux distribution. This could be for example the polynomial degree for the fitting approach or the smoothing length for the local polynomial regression. The systematic errors are similar in size for all measurements, but the temperature differences across the axial length of the cylinder depend on the heat transfer and whether the cylinder is cooled or not. The necessary approach needs to adapt to the temperature differences and the measurement errors to produce useful heat flux distributions. A fixed value for these parameters is therefore not applicable. An approach, where the parameters were set using a crossvalidation method yielded better but still not satisfactory results. Some data sets were still noisy after the correction was applied while others were smoothed to much leading to a loss in heat transfer information. Another disadvantage of the common approaches is that a symmetry condition is difficult to superimpose. This is why a new correction algorithm is presented hereafter, overcoming the stated challenges.

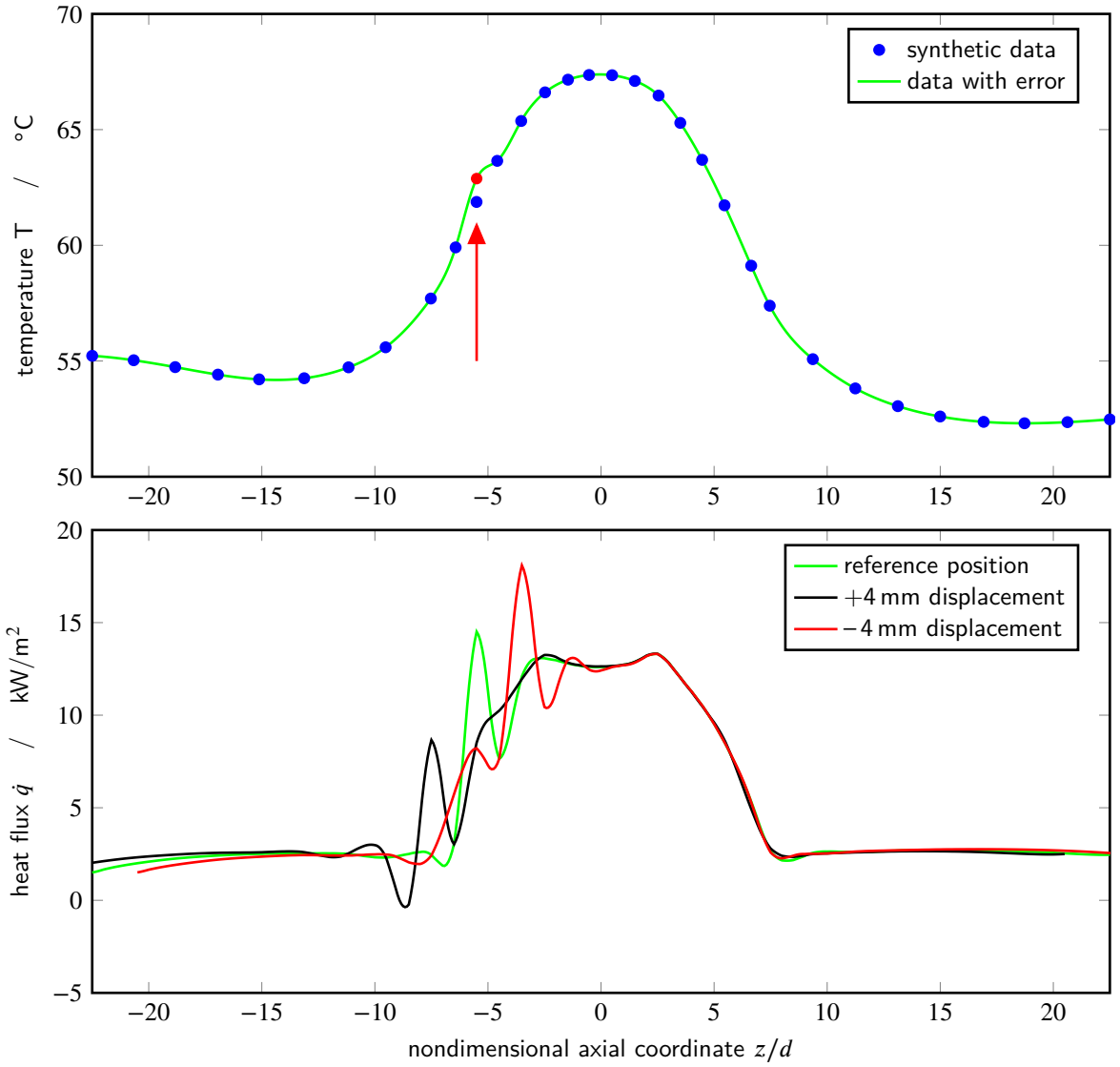


Figure 3: Top: Temperature data for synthetic data set at thermocouple locations for reference nozzle position (blue), interpolated data with additional measurement error of 1 K at eleventh thermocouple from the left (green); Bottom: Calculated heat flux for the three axial positions: reference (green), positive nozzle displacement (blue) and negative nozzle displacement (red)

The heat flux for the three measurements at different axial locations of impingement should be identical, just shifted by the known distance of the nozzle movement. Additionally, the heat flux is assumed to be symmetrical with respect to the impingement point. A systematic measurement error of one of the thermocouples results in a spike in heat flux for all three measurements but at different distances with respect to the impingement point because of the axial movement of the nozzle. This is illustrated in the bottom part of Fig. 3 with the three spikes in heat flux stemming from the synthetic +1 K measurement error that has been added to the data set. A positive measurement error, which means a temperature reading higher than the true temperature, results in a positive spike in heat flux, a negative error in a negative spike. This error also affects the adjacent thermocouples in the opposite sense, meaning a smaller negative spike in heat flux for a positive error and vice versa. This is also observable in Fig. 3, where each positive peak imposes smaller negative peaks at adjacent thermocouple locations.

The new correction algorithm to overcome the problem of systematic measurement errors is based on the three measurements of the same operating condition but with different axial positions of impingement. This way, systematic errors, i.e. measurement errors linked to individual thermocouples, can be drastically reduced. An average of the temperatures of the three measurements is not possible since the finite length of the rotor has an influence on the temperature of the side walls. The only way to overcome this problem is to use the heat flux

instead of the measured temperatures on which the finite length of the rotor has only a negligible effect. Additionally, axial symmetry with respect to the impingement point is assumed. All six calculated heat fluxes (3 axial nozzle positions times two for the symmetry) with the same distance to the impingement point are averaged and used as the reference heat flux distribution. The three heat fluxes calculated for each thermocouple are then compared to their respective reference heat flux. If all three heat fluxes are either above or below the reference heat flux, a systematic error is highly probable and, therefore, assumed. Otherwise, no systematic error is assumed and the temperature remains unaltered. Also, no change is done to the thermocouples furthest away from the impingement point where there are no six heat fluxes for the reference heat flux distribution, resulting in the last three thermocouples to either side remaining unaltered. The minimum absolute value of the three heat flux differences is taken as the indicator on how much the temperature for the respective thermocouple is corrected. Each indicator is multiplied by a factor of $10^{-4}\ K\,m^2/W$ to obtain the temperature correction for each thermocouple. This value is chosen because it minimizes the number of iterations necessary while at the same time avoiding diverging behavior. Additionally, to prevent the introduction of a bias, the sum of all corrections has to equal zero. Hence, the temperature corrections are weighted such that this criterion is met. The entire process is repeated 50 times with an update for the temperature distribution after each iteration. The resulting temperature distribution is smoother which means the resulting heat fluxes show a significantly better signal-to-noise ratio without distorting the data. The corrected temperature and heat flux distribution are plotted in Fig. 2 in green. Although the changes in temperature at each specific measurement location remains small (<1.5 K), the resulting heat flux distribution is not only more symmetrical but exhibits a significantly lower noise level.

The data correction is only applied to the thermocouples on the outside surface, not the ones on the inside surface. Although these inner thermocouples might also show systematic measurement errors, the assumptions made in the derivation of the algorithm do not hold up. Neither the symmetry assumption nor the translation assumption of the heat flux by the nozzle movement are fulfilled. Small measurement errors on the inside surface within the bounds of the uncertainty of the thermocouples, however, do not distort the heat flux distribution on the outside surface. Thermal diffusion (heat conduction) between the inside and outside surfaces smooths out any local measurement errors. Additionally, the distance between the thermocouples on the inside surface (10 mm) is large enough such that the effect described in figure Fig. 3 is greatly reduced. A systematic error of all inside thermocouples in positive or negative direction would change the overall heat transfer. Similar to the outside surface, such an improbable case is neglected since it would not be distinguishable from an actual physical effect. Therefore, no data correction is necessary for the 10 thermocouples on the inside surface of the cylinder.

### 3.4 Evaluation

The evaluated heat flux from the previous section can be used to calculate the heat transfer coefficient

$$h = \frac{\dot{q}}{T_\mathrm{w} - T_\mathrm{aw}}\,. \tag{3}$$

The driving temperature difference is defined as the difference between the wall temperature $T_\mathrm{w}$ and the adiabatic wall temperature $T_\mathrm{aw}$. Subsequently, the Nusselt number can be deduced

$$\mathrm{Nu} = \frac{h\,d}{k_\mathrm{oil}}\,, \tag{4}$$

with $d$ being the jet diameter and $k_\mathrm{oil}$ being the thermal conductivity of the oil at oil jet temperature.

The adiabatic wall temperature is usually derived from the recovery factor and the kinetic energy of the oil jet. The recovery factor itself is mainly a function of Prandtl number, jet velocity profile and radial distance to the impingement point [23]. The adiabatic wall temperature can significantly exceed the oil jet temperature for high Prandtl number fluids because of the heat dissipation in the boundary layer [24]. As there is no literature available for a free surface liquid jet of high Prandtl number impinging on a moving surface, the recovery factor cannot simply be calculated. Therefore, the adiabatic wall temperature has to be measured during the experiments. A direct measurement is only possible with a rotor of high thermal resistance to fulfill the adiabatic wall boundary condition. Unfortunately, although the thermal conductivity of the rotor is small compared to other metals, it is too large for an acceptable direct measurement.

The superposition principle is applied instead to obtain the adiabatic wall temperature through the combined evaluation of two separate measurements. As long as the material properties of the oil remain close to constant in the boundary layer, the energy equation for the fluid flow simplifies to a linear function. This allows for a superposition of different particular solutions to obtain the adiabatic wall temperature [25, 26]. A schematic of the principle can be seen in Fig. 4. Two measurements, one with high heat flux and one with low heat

flux, are performed for the same operating condition. This implies that the oil jet and its flow behavior remain unchanged, whereas the inside of the cylinder is either cooled or thermally insulated. As depicted in Fig. 4, the linear superposition is used to calculate to the adiabatic wall temperature (x-intercept) as well as the heat transfer coefficient (negative slope).

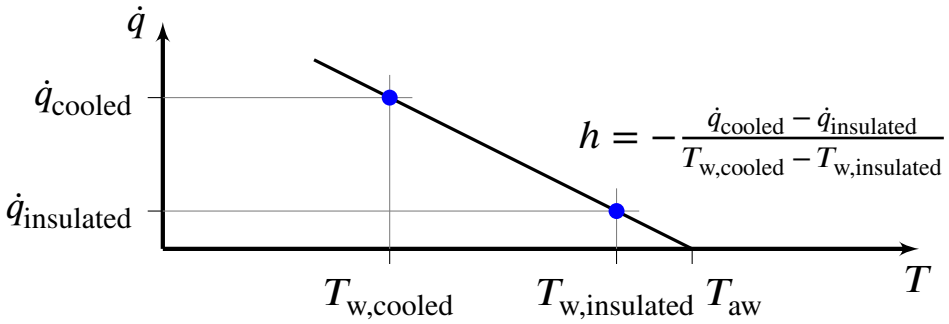


Figure 4: Schematic of the superposition principle adopted from Kneer [27]

The requirement that the fluid flow remains unchanged between the two measurements (cooled and insulated) can be fulfilled by keeping the operating conditions the same. However, the same requirement cannot be met for the air inside the test chamber. The reference air temperature increases significantly when the air cooling on the inside of the cylinder is turned off. This means that the superposition principle is not applicable to the areas where air is in contact with the cylinder surface. Because there are no direct measurements available so far to distinguish between air and oil present on the cylinder surface, an assumption is made. Oil is assumed to be present whenever the heat transfer coefficient is above a certain threshold: $h > 250\,\text{W/m}^2\,\text{K}$. This value is chosen because it is above the convective heat transfer for air at the highest rotational speeds, therefore, limiting the superposition to the area where oil is in contact with the cylinder surface. The second assumption made in the evaluation process is that the adiabatic wall temperature is independent of the distance to the impingement point. Although such a dependence is possible, no clear evidence is found in the measurement data. Thus, a constant adiabatic wall temperature is assumed for each operating condition.

A linear regression (see Fig. 4) is fitted to each position on the cylinder, excluding those where the heat transfer coefficient falls below the threshold of $h \leq 250\,\text{W/m}^2\,\text{K}$. Additionally, the x-intercept (the adiabatic wall temperature) is kept constant. A total of 12 points are used for each position (distance to the impingement point). These 12 points stem from the multiplication of 3 axial measurements times 2 for the symmetry times 2 for the cooled and insulated measurement at the same operating condition. The regression is repeated with an adiabatic wall temperature chosen from the interval between $T_{\text{jet}} - 2\,\text{K}$ and $T_{\text{jet}} + 10\,\text{K}$ with a step size of 0.1 K. The linear regression with the best fit ($r^2$-value) is chosen as the final result. Each operating condition (flow rate, rotational speed and oil temperature) yields one adiabatic wall temperature and a Nusselt number distribution over the axial coordinate. These results will be presented in the following section.

# 4.0 RESULTS

With the experiments and the data correction algorithm in place, the experimental data is evaluated and compared in this section. A small parameter study is performed to identify the influence of the input parameters on the heat transfer. A total of 8 different measurements are completed with their corresponding operating conditions listed in Table 2. The operating conditions are chosen to be able to identify the effect of one parameter variation while holding the other parameters constant. Each operating condition was measured six times (cooled/insulated times three axial nozzle positions) and evaluated simultaneously as a single data set (see section Section 3).

## 4.1 Dissipation Effect

Heat dissipation inside the oil film increases the adiabatic wall temperature. This only becomes relevant for high Prandtl number fluids such as the oil in this study. The Prandtl number of the oil jet is listed in Table 2 as well as the temperature increase. The reason for the temperature increase is the heat dissipation inside the hydraulic boundary layer. It significantly increases the oil temperature at the edge of the thermal boundary layer with the latter being much smaller than the hydraulic one because of the high Prandtl number. This increase in temperature at the edge of the thermal boundary layer corresponds to the described increase in adiabatic wall

temperature. All values in the last column are positive except for measurement number 7, for which a negligible negative difference of $\Delta T_{\mathrm{aw,jet}} = T_{\mathrm{aw}} - T_{\mathrm{jet}} = -0.1\,\mathrm{K}$ is evaluated. On the one hand, the parameters oil flow rate and oil jet temperature might have a small influence on the adiabatic wall temperature. However, these effects are too small to be conclusive. On the other hand, a strong influence of the rotational speed on the adiabatic wall temperature is clearly observable. The dissipation effect in the boundary layer leads to a temperature increase of up to $\Delta T_{\mathrm{aw,jet}} = 3.7\,\mathrm{K}$. All measurements follow this trend, however, several more measurements are needed to deduce a correlation for the temperature increase caused by heat dissipation.

The uncertainty of the temperature increase is directly tied to and can be approximated by the accuracy of the isolated temperature measurement. Even though the uncertainty of a single thermocouple in these measurements is $\Delta T = \pm 1.5\,\mathrm{K}$, the average measurement error is significantly lower. The temperature corrections, the average over time and the spatial average for the temperature increase all decrease the measurement uncertainty (see Section 3). It is, therefore, assumed that the uncertainty is below 1.5 K.

The heat dissipation is independent of the direction of the heat transfer. Therefore, the adiabatic wall temperature will always be above the oil jet temperature, no matter if the oil jet cools or heats the cylinder. The consequences of the dissipation effect are, however, different for the two application cases. For the case of an oil jet heating the cylinder, the temperature increase caused by dissipation increases the driving temperature difference ($T_{\mathrm{aw}} - T_{\mathrm{w}}$). Hence, dissipation increases the heat transfer from oil to cylinder. For the case of an oil jet cooling a cylinder, the case close to the application in an aero engine gearbox, the dissipation effect decreases the driving temperature difference and, therefore, the heat transfer. The dissipation effect has to be taken into account and reduced as much as possible in the design process for such applications, especially for low driving temperature differences between oil jet and cylinder.

## 4.2 Oil Flow Rate

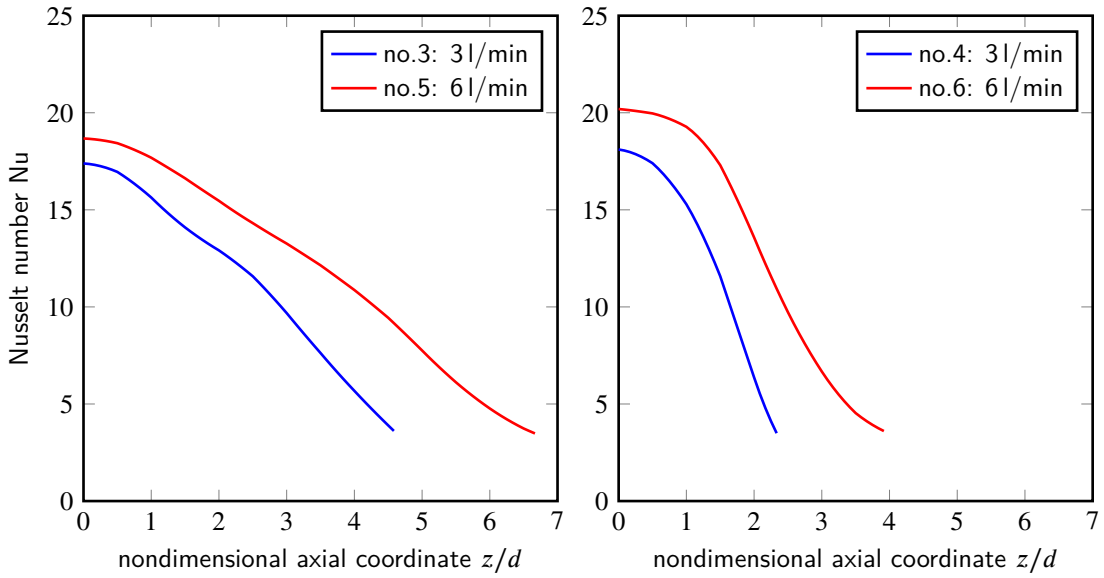


Figure 5: Left: Nusselt number distribution for $T_{\mathrm{oil}} = 80°\mathrm{C}$ and 2000 rpm and different oil flow rates ; Right: Nusselt number distribution for $T_{\mathrm{oil}} = 80°\mathrm{C}$ and 6200 rpm and different oil flow rates

Table 2: Operating conditions for the measurements

| no. | $T_{\mathrm{jet}}$ [°C] | oil flow rate [l/min] | rotational speed [rpm] | Pr [-] | $\Delta T_{\mathrm{aw,jet}}$ [K] |
|---|---|---|---|---|---|
| 1 | 60 | 3 | 2000 | 178.31 | 0.4 |
| 2 | 60 | 3 | 6200 | 178.31 | 3.7 |
| 3 | 80 | 3 | 2000 | 105.29 | 0.5 |
| 4 | 80 | 3 | 6200 | 105.29 | 3.7 |
| 5 | 80 | 6 | 2000 | 105.29 | 0.8 |
| 6 | 80 | 6 | 6200 | 105.29 | 3.7 |
| 7 | 100 | 3 | 2000 | 68.82 | −0.1 |
| 8 | 100 | 3 | 6200 | 68.82 | 3.4 |

The first parameter varied in the parameter study is the oil flow rate. Two comparisons can be drawn, which are plotted in Fig. 5 as a function of Nusselt number over axial coordinate. On the left hand side, the increase of the oil flow rate from 3 to 6 l/min for a constant rotational speed of 2000 rpm is shown, whereas on the right hand side, the same increase in oil flow rate is depicted for 6200 rpm. In both cases, the oil jet temperature is kept constant at 80°C. The increase in oil flow rate widens the oil film in the axial direction. This can be explained by the higher momentum upon impingement. Additionally, the Nusselt number increases with oil flow rate. This might also be attributed to the increase in momentum, leading to a higher jet Reynolds number. All measurements show a monotonically decreasing Nusselt number with increasing axial distance to the impingement point. This follows the trend described in the literature, where the heat transfer decreases with the growing boundary layer away from the impingement point. All Nusselt number distributions end at approximately Nu=4, which is where the threshold $h = 250\,\mathrm{W/m^2\,K}$ is crossed. This marks the axial limit of the oil film and, therefore, the limit of the superposition based evaluation. It can be concluded that increasing oil flow rate increases the width of the oil film as well as the heat transfer at every location in the oil film.

### 4.3 Oil Temperature

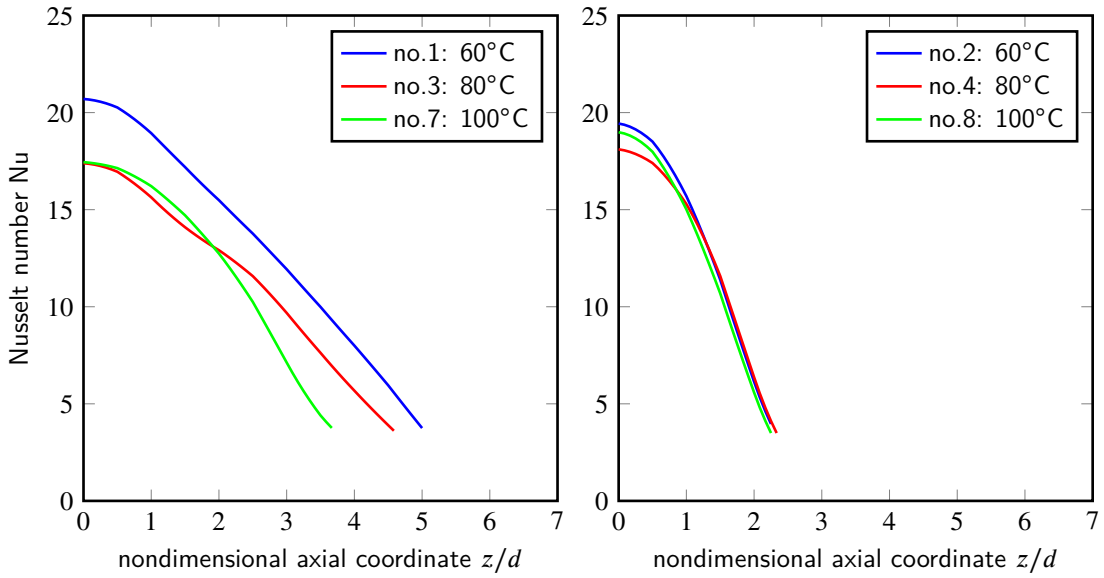


Figure 6: Left: Nusselt number distribution for 3 l/min and 2000 rpm and different oil jet temperatures; Right: Nusselt number distribution for 3 l/min and 6200 rpm and different oil jet temperatures

The oil temperature significantly influences the viscosity of the oil according to the following equation by Glahn [28]

$$\nu = \left(10^{10^{8.962182-3.527033\,log_{10}(T)}} - 0.8\right)\frac{\mathrm{mm}^2}{\mathrm{s}}\,. \tag{5}$$

An increase in oil temperature leads to a decrease in oil viscosity and subsequently in Prandtl number. In the temperature range of the experiments (60°C-100°C), this results in a reduction in Prandtl number by more than 60 % (see Table 2). All other oil properties remain fairly constant over that temperature range: density (-5 %), specific heat (+6 %), thermal conductivity (-1 %), thermal diffusivity (-2 %) and surface tension (-18 %). Although the changes of those oil properties may also contribute to a change in heat transfer, it is assumed that the change in viscosity is the dominant factor when varying the oil temperature. This is in accordance with the literature on oil jet cooling on static surfaces, which emphasizes that the Reynolds and Prandtl number as the main parameters with respect to heat transfer [9, 24]. Both of those dimensionless numbers are affected by viscosity.

A change in oil temperature does not seem to have an effect on the Nusselt number distribution for high rotational speeds of 6200 rpm, as can be seen on the right hand side of Fig. 6. This could be explained by the high surface speed of the cylinder and the resulting small axial width of the oil film. The oil viscosity might only have a limited effect in the area near the impingement point, which is why the results are so close together. For lower rotational speeds of 2000 rpm, the oil viscosity can influence the flow behavior. Counterintuitively, the oil film widens and the heat transfer increases with increasing viscosity. More data is needed for a conclusive

explanation. To conclude, the viscosity of the oil does not seem to have an effect on the heat transfer for high rotational speeds but might have a small effect for low rotational speeds.

### 4.4 Rotational Speed

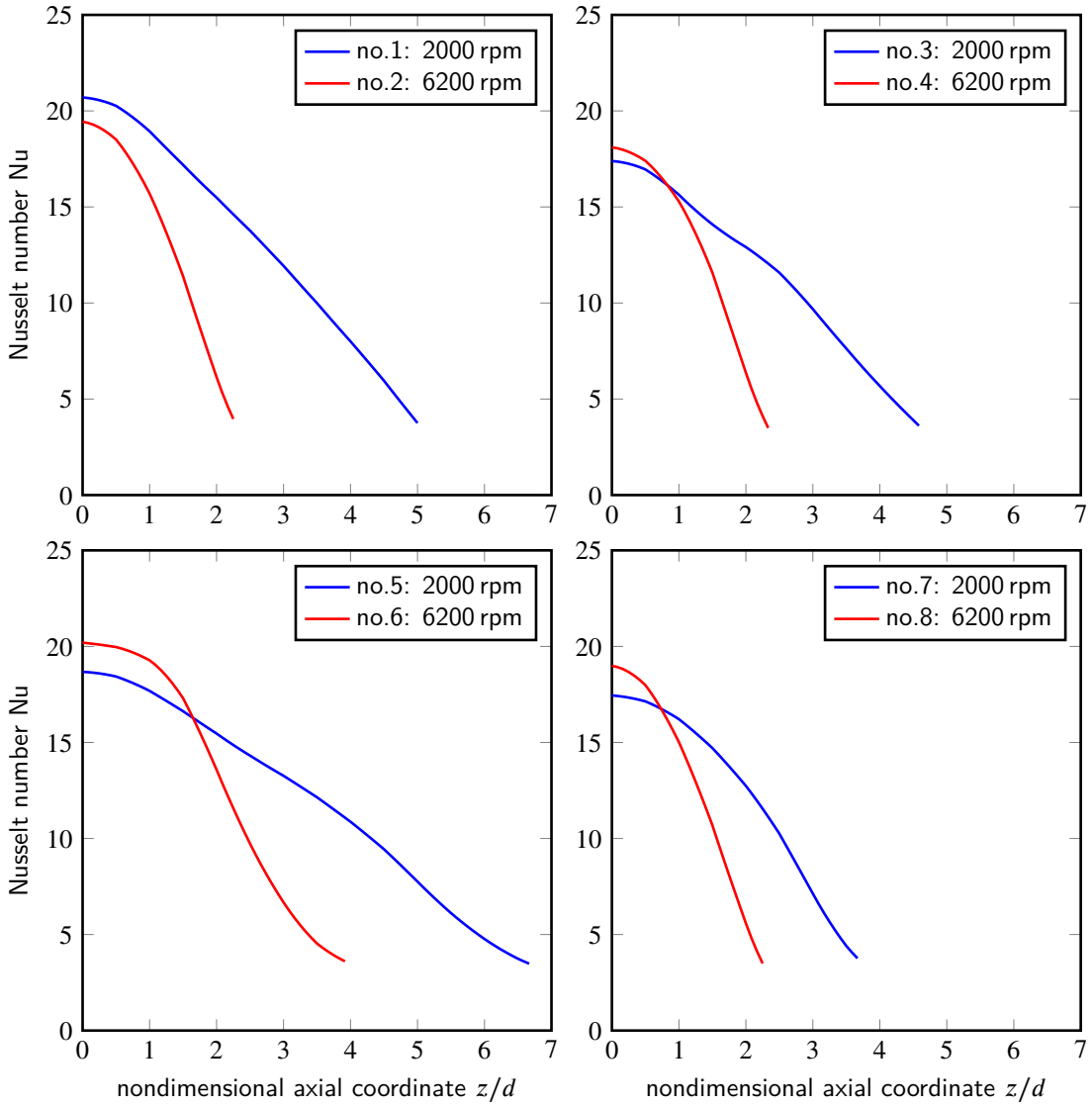


Figure 7: Nusselt number distributions for 60°C and 3 l/min (top left), 80°C and 3 l/min (top right), 80°C and 6 l/min (bottom left) and 100°C and 3 l/min (bottom right)

The main influence of the rotational speed on the Nusselt number distribution is the change in oil film width. An increase in rotational speed significantly decreases the oil film width. This is observed in Fig. 7 in all four plots. This behavior can be explained by the increase in surface speed. Higher surface speeds accelerate the oil faster in the tangential direction after impingement and fling the oil off the surface quicker. Thus, the oil has less time to spread in the axial direction, reducing the axial width of the oil film. The maximum Nusselt number at the impingement point increases slightly with rotational speed except for the 60°C case in the top left plot. These increases are still within the limits of measurement uncertainty and no clear trend is observable.

## 5.0 SUMMARY

An experimental test rig at the Institute of Thermal Turbomachinery is modified to enable oil jet impingement measurements on a rotating cylinder. Temperature measurements along the surface of the cylinder are recorded for different oil flow rates, oil jet temperatures and rotational speeds. The calibrated and time-averaged tempera-

ture data is then corrected to minimize the effect of small systematic measurement errors within the measurement uncertainty of the used thermocouples. This new algorithm enhances the signal-to-noise ratio and, therefore, allows for a more accurate evaluation of the heat transfer data. The results show a strong influence of the rotational speed on the dissipation in the boundary layer. Increasing the rotational speed increases adiabatic wall temperature to values up to 3.7 K above the oil jet temperature. Such a strong effect needs to be taken into accounted, especially if the heat transfer information is to be used for cooling applications. The results show an increase in heat transfer with increasing oil flow rate, while an increase in rotational speed decreases the width of the oil film and thus limits the heat transfer to a narrower region. The oil jet temperature and the corresponding oil viscosity do not seem to have a significant effect on the heat transfer. With the present study, an evaluation procedure is established to gain insight into the complex heat transfer process for an oil jet impinging on a rotating cylinder. Further measurements are needed to establish a correlation for the adiabatic wall temperature and the Nusselt number. The results of this study can be transferred to the application of the oil jet cooling of gears as present in geared turbofan engines. The study contributes to the development of a more efficient lubrication and cooling system in new gearbox designs.

## 6.0 ACKNOWLEDGEMENTS

The research leading to the results presented in this paper is supported by the Deutsche Forschungsgemeinschaft (DFG project number 437324525). This financial support is gratefully acknowledged. The authors wish to thank Pascal Nguyen and Nils Horneff for supporting the data acquisition activities carried out at the Institute of Thermal Turbomachinery. The responsibility of the content lies solely with the authors.

## References

[1] Kromer, C., Cordes, L., Keller, M. C., et al. 2019. Analytical Solution to the Heat Transfer in Fling-off Cooling of Spur Gears. *Journal of Heat Transfer*

[2] Kromer, C., von Plehwe, F. C., Cordes, L., et al. 2019. “Heat Transfer by Impingement Cooling of Spur Gears”. In: *Proceedings of the 68th German Aerospace Congress (DLRK), Darmstadt, Germany, September 30 - October 2, 2019*. DOI: 10.25967/490085

[3] Kromer, C., Plehwe, F. C. von, Keller, M. C., et al. 2020. “Analytical model for the heat transfer in impingement cooled spur gears”. In: *Turbo Expo: Power for Land, Sea, and Air*, V001T01A023. ISBN 0791884058

[4] Keller, M. C., Schwitzke, C., and Bauer, H.-J. 2018. Numerische Simulation der Ölstrahl-Zahnrad-Interaktion bei Flugtriebwerken mit hohem Nebenstromverhältnis: Stand der Forschung. DOI: 10.5445/IR/1000085339

[5] Keller, M. C., Braun, S., Wieth, L., et al. 2019. Smoothed Particle Hydrodynamics Simulation of Oil-jet Gear Interaction. *Journal of Tribology* 141.7. DOI: 10.1115/1.4043640

[6] Keller, M. C., Kromer, C., Cordes, L., et al. 2019. “Effect of Design Parameters on Oil-jet Gear Interaction”. In: *Proceedings of ISABE 2019, Melbourne, Australia, 22-27 September, 2019*

[7] Plehwe, F. C. von, Schwitzke, C., and Bauer, H.-J. 2021. Heat Transfer Coefficient Distribution on Oil Injection Cooled Gears: Experimental Method, Uncertainty, and Results. *Journal of Tribology* 143.9. ISSN 0742-4787

[8] Ayan, E., Plehwe, F. C. von, Keller, M. C., et al. 2020. “Experimental Determination of Heat Transfer Coefficient on Impingement Cooled Gear Flanks: Validation of the Evaluation Method”. In: *Turbo Expo: Power for Land, Sea, and Air*, V05BT13A004. ISBN 0791884988

[9] Webb, B. W. and Ma, C.-F. 1995. Single-Phase Liquid Jet Impingement Heat Transfer. In: *Advances in Heat Transfer*. Ed. by Hartnett, J. P., Irvine, T. F., and Cho, Y. I. Vol. 26. Advances in Heat Transfer. s.l., pp. 105–217. DOI: 10.1016/S0065-2717(08)70296-X

[10] Ma, C. F., Sun, H., Auracher, H., et al., eds. 1990. Local convective heat transfer from vertical heated surfaces to impinging circular jets of large Prandtl number liquids. Vol. 2

[11] Carper, H. J., Saavedra, J. J., and Suwanprateep, T. 1986. Liquid Jet Impingement Cooling of a Rotating Disk. *Journal of Heat Transfer* 108.3. Pages 540. DOI: 10.1115/1.3246968

[12] Keshavarz, B., Green, S. I., Davy, M. H., et al. 2011. Newtonian liquid jet impaction on a high-speed moving surface. *International Journal of Heat and Fluid Flow* 32.6. Pages 1216–1225. DOI: 10.1016/j.ijheatfluidflow.2011.08.001

[13] Keshavarz, B., Green, S. I., and Eadie, D. T. 2012. Elastic liquid jet impaction on a high-speed moving surface. *AIChE Journal* 58.11. Pages 3568–3577. DOI: 10.1002/aic.13737

[14] Keshavarz, B., Green, S. I., Davy, M. H., et al. 2010. "Newtonian Airless Liquid Jet Interaction with a High Speed Moving Surface". In: *23rd Annual Conference on Liquid Atomisation and Spray Systems*. Brno

[15] Moulson, J. B. T. and Green, S. I. 2013. Effect of ambient air on liquid jet impingement on a moving substrate. *Physics of Fluids* 25.10. Pages 102106. DOI: 10.1063/1.4823726

[16] Guo, Y. and Green, S. 2015. Visualization of high speed liquid jet impaction on a moving surface. *Journal of visualized experiments : JoVE* 98. DOI: 10.3791/52603

[17] Rahmani, H., Vakil, A., and Green, S. I. 2016. Numerical Simulation of a Liquid Jet Impinging on a Moving Substrate

[18] Fujimoto, H., Suzuki, Y., Hama, T., et al. 2011. Flow Characteristics of Circular Liquid Jet Impinging on a Moving Surface Covered with a Water Film. *ISIJ International* 51.9. Pages 1497–1505. DOI: 10.2355/isijinternational.51.1497

[19] Fujimoto, H., Lee, Y., Kato, R., et al. 2013. Experimental and numerical study of twin circular water jets impinging on a moving thin film. *ISIJ International* 53.8. Pages 1427–1435. ISSN 0915-1559

[20] Zumbrunnen, D. A. 1991. Convective heat and mass transfer in the stagnation region of a laminar planar jet impinging on a moving surface. *Journal of Heat Transfer* 113.3. Pages 563–570. ISSN 00221481

[21] Deem, H. W., Wood, W. D., and Lucks, C. F. 1958. Transactions of the Metallurgical Society of AIME. v212

[22] Umezawa, O. and Ishikawa, K. 1992. Cryogenics. v32. Vol. No. 10

[23] Ma, C. F., Zheng, Q., and Ko, S. Y. 1997. Local heat transfer and recovery factor with impinging free-surface circular jets of transformer oil. *International Journal of Heat and Mass Transfer* 40.18. Pages 4295–4308. ISSN 00179310

[24] Ma, C. F., ed. 2002. Impingement heat transfer with meso-scale fluid jets

[25] Metzger, D. E., Carper, H. J., and Swank, L. R. 1968. Heat transfer with film cooling near nontangential injection slots. *0022-0825*. ISSN 0022-0825

[26] Choe, H., Kays, W. M., and Moffat, R. J., eds. 1974. The superposition approach to film-cooling

[27] Kneer, J. 2017. Zur Interaktion von Filmkühlung und Heißgasströmung auf konturierten Turbinenseitenwänden. Vol. 69. ISBN 3832546383

[28] Glahn, A. 1995. Zweiphasenströmung in Triebwerkslagerkammern - Charakterisierung der Ölfilmströmung und des Wärmeübergangs. Dissertation. Karlsruhe: Universität Karlsruhe